

THE ABUNDANCE OF STAR-FORMING GALAXIES IN THE REDSHIFT RANGE 8.5 TO 12: NEW RESULTS FROM THE 2012 HUBBLE ULTRA DEEP FIELD CAMPAIGN

RICHARD S ELLIS¹, ROSS J MCLURE², JAMES S DUNLOP², BRANT E ROBERTSON³, YOSHIKI ONO⁴, MATTHEW A SCHENKER¹, ANTON KOEKEMOER⁵, REBECCA A A BOWLER², MASAMI OUCHI⁴, ALEXANDER B ROGERS², EMMA CURTIS-LAKE², EVAN SCHNEIDER³, STEPHANE CHARLOT⁷, DANIEL P STARK³, STEVEN R FURLANETTO⁶, MICHELE CIRASUOLO^{2,8}

Draft version October 29, 2018

ABSTRACT

We present the results of the deepest search to date for star-forming galaxies beyond a redshift $z \simeq 8.5$ utilizing a new sequence of near-infrared Wide Field Camera 3 images of the Hubble Ultra Deep Field. This ‘UDF12’ campaign completed in September 2012 doubles the earlier exposures with WFC3/IR in this field and quadruples the exposure in the key F105W filter used to locate such distant galaxies. Combined with additional imaging in the F140W filter, the fidelity of high redshift candidates is greatly improved. Using spectral energy distribution fitting techniques on objects selected from a deep multi-band near-infrared stack we find 7 promising $z > 8.5$ candidates. As none of the previously claimed UDF candidates with $8.5 < z < 10$ is confirmed by our deeper multi-band imaging, our campaign has transformed the measured abundance of galaxies in this redshift range. Although we recover the candidate UDFj-39546284 (previously proposed at $z=10.3$), it is undetected in the newly added F140W image, implying it lies at $z=11.9$ or is an intense emission line galaxy at $z \simeq 2.4$. Although no physically-plausible model can explain the required line intensity given the lack of Lyman α or broad-band UV signal, without an infrared spectrum we cannot rule out an exotic interloper. Regardless, our robust $z \simeq 8.5 - 10$ sample demonstrates a luminosity density that continues the smooth decline observed over $6 < z < 8$. Such continuity has important implications for models of cosmic reionization and future searches for $z > 10$ galaxies with JWST.

Subject headings: cosmology: reionization — galaxies: evolution — galaxies: formation — galaxies: stellar content

1. INTRODUCTION

Good progress has been achieved in exploring the latest frontier in cosmic history, namely the 700 Myr period corresponding to the redshift interval $6 < z < 15$. During this time, star-forming galaxies likely played a significant role in completing the reionization of intergalactic hydrogen (Robertson et al. 2010a; Bromm & Yoshida 2011; Dunlop 2012). Inevitably, our census of galaxies during this era is limited by our current observational facilities. Most progress has been made in the lower redshift range $6 < z < 8.5$ via deep imaging with the *Hubble Space Telescope* (HST). This has revealed several hundred star-forming galaxies and a dominant contribution to the luminosity density from low luminosity examples (Oesch et al. 2010; McLure et al. 2011; Bouwens et al. 2010, 2012a). Measures of the assembled stellar mass from *Spitzer Space Telescope* photometry at $z \simeq 5-6$ (Stark et al. 2007a; Eyles et al. 2007; González et al. 2010, 2011; Labbé et al. 2012) suggest that

star formation extended to redshifts well beyond $z \simeq 8$ but there has been limited progress in finding these earlier, more distant, sources.

Various groups have attempted to find $z > 8.5$ galaxies using the well-established technique of absorption by intervening neutral hydrogen below the wavelength of Lyman α . A redshift $z=8.5$ represents a natural frontier corresponding to sources which progressively ‘drop out’ in the HST Y-band F105W and J-band F125W filters. Bouwens et al. (2011) and Yan et al. (2010) used data from the campaign completed in 2009 with the near-infrared Wide Field Camera 3 (WFC3/IR) in the Hubble Ultra Deep Field (GO 11563, PI: Illingworth, hereafter UDF09). Bouwens et al. initially located 3 promising J-band dropouts at $z \simeq 10$ but, on re-examining the completed dataset, presented only a single candidate, UDFj-39546284 at a photometric redshift of $z=10.3$, not drawn from the original three. Bouwens et al. also found 3 sources in the interval $8.5 < z < 9$, robustly detected in F125W with (F105W - F125W) colors implying a Lyman break near the red edge of the F105W filter. In marked contrast, Yan et al. presented a list of 20 faint J-band dropout candidates arguing all had redshifts $z > 8.5$. However, none of the Yan et al. and Bouwens et al. candidates are in common. Gravitational lensing by foreground clusters of galaxies can overcome some of the difficulties associated with deep imaging of blank fields. Such sources can be magnified by factors of $\times 5-30$ ensuring more reliable photometry (Richard et al. 2011). In favorable cases, their multiply-imaged nature offers a lower limit on their angular diameter distance (Ellis et al. 2001; Kneib et al. 2004). The CLASH HST survey (GO 12065 - 12791, PI: Postman) has discovered sev-

¹ Department of Astrophysics, California Institute of Technology, MS 249-17, Pasadena, CA 91125; rse@astro.caltech.edu

² Institute for Astronomy, University of Edinburgh, Royal Observatory, Edinburgh EH9 3HJ, UK

³ Department of Astronomy and Steward Observatory, University of Arizona, Tucson AZ 85721

⁴ Institute for Cosmic Ray Research, University of Tokyo, Kashiwa City, Chiba 277-8582, Japan

⁵ Space Telescope Science Institute, Baltimore, MD 21218

⁶ Department of Physics & Astronomy, University of California, Los Angeles CA 90095

⁷ UPMC-CNRS, UMR7095, Institut d’Astrophysique de Paris, F-75014, Paris, France

⁸ UK Astronomy Technology Centre, Royal Observatory, Edinburgh EH9 3HJ, UK

eral such $z > 8.5$ candidates, three at $z \simeq 9-10$ (Zheng et al. 2012; Bouwens et al. 2012b) and a multiply-imaged source at $z=10.7$ (Coe et al. 2012).

A key issue is the uncertainty in converting the various detections into estimates of the abundance of galaxies beyond $z \simeq 8$. Bouwens et al. (2011, see also Oesch et al. (2012)) claimed that their detection of a single $z \simeq 10.3$ candidate in the UDF09 campaign implies a shortfall of a factor $\simeq 3-6$ compared to that expected from the declining star formation rate density over $6 < z < 8$. This could imply the growth of activity was particularly rapid during the 200 Myr from $z \simeq 10$ to 8. However, Coe et al. (2012) claim the CLASH detections are consistent with a continuous decline to $z \simeq 10.7$. One limitation of the lensing strategy as a means of conducting a census (rather than providing individual magnified sources for scrutiny) is the uncertainty associated with estimating the survey volume which depends sensitively on the variation of magnification with position across the cluster field (c.f., Santos et al. 2004; Stark et al. 2007b).

There are several drawbacks with the earlier UDF09 campaign with respect to conducting a census of $z > 8.5$ galaxies. Limiting factors in considering the robustness of the faint candidates include the poor signal to noise in subsets of the F160W data, the reliance on only a single detection filter and the limited depth of the critical F105W imaging data whose null detection is central to locating $z > 8.5$ candidates.

This article heralds a series that presents results from a deeper UDF campaign with WFC3/IR completed in September 2012 (GO 12498, PI; Ellis, hereafter UDF12) which remedies the above deficiencies by (i) substantially increasing the depth of the F105W image (by $\times 4$ in exposure time) essential for robust rejection of $z < 8.5$ sources, (ii) increasing the depth of the detection filter F160W (a 50% increase in exposure time) and (iii) adding a deep image in the F140W filter matching the depth now attained in F160W. This filter partially straddles the F125W and F160W passbands offering valuable information on all $z > 7$ sources, the opportunity for an independent detection for $8.5 < z < 10.5$ sources and the first dropout search beyond $z \simeq 10.5$.

The UDF12 survey depths (including UDF09) in the various filters are summarized in Table 1. Our aim, achieved in full, has been to match the depths in F125W, F140W, and F160W for unbiased high redshift galaxy detection, and to reach 0.5 mag deeper in F105W to ensure a $2\text{-}\sigma$ limit 1.5 mag deeper than the $5\text{-}\sigma$ limit in the longer wavelength bands. Further details of the survey and its data reduction are provided in Koekemoer et al. (2012) and catalogs of $z \simeq 7$ and 8 sources used to estimate the luminosity function are presented in complementary articles by Schenker et al. (2012) and McLure et al. (2012). The spectral properties of the high-redshift UDF12 sources are measured and analyzed by Dunlop et al. (2012). A review of the overall implications of the survey in the context of cosmic reionization is provided in Robertson et al. (2012). Public versions of the final reduced WFC3/IR UDF12 images, incorporating additions of all earlier UDF data, are available to the community on the team web page⁹. All magnitudes are in the AB system (Oke 1974).

⁹ <http://udf12.arizona.edu/>

2. STAR FORMING GALAXIES WITH $Z > 8.5$

To select $z > 8.5$ candidates, we examined the stacked combination of the 80 orbit F160W (UDF12 plus UDF09), 30 orbit F140W (UDF12) and 34 orbit F125W (UDF09) images and located all sources to a 5σ limit within filter-matched apertures of $0.4 - 0.5$ arc sec corresponding to $m_{AB} \simeq 29.9-30.1$. Making effective use of our new ultra-deep 93 orbit (71 from UDF12, 22 from UDF09) F105W image and the deep ACS photometry, we utilized the SED approach discussed in McLure et al. (2010, 2011) to derive photometric redshifts of all such sources. Seven convincing $z > 8.5$ candidates were found. An independent search using the same master sample selecting those which drop out in F105W (2σ rejection corresponding to $m_{AB} > 31.0$) and no detection (2σ) in a combined ACS *BViz* stack delivered the same $z > 8.5$ candidates. All sources but one (see below) are detected in more than one filter and all are detected with an appropriately-reduced signal/noise in time-split subsets over the collective UDF09 and UDF12 campaigns. Figure 1 shows HST broad-band images for these 7 sources. Their SED fits and redshift probability distributions $p(z)$ are given in Figure 2. Identifications, source photometry and optimum redshifts are summarized in Table 1.

The great advantage of the SED fitting approach is that it allows us to quantify the possibility of alternative low-redshift solutions. Four of our 7 objects (UDF12-3921-6322, UDF12-4265-7049, UDF12-4344-6547 & UDF12-3947-8076) have low probabilities of being at $z < 4$ (1–4%). UDF12-4106-7304 has a $\simeq 10\%$ probability for $z < 4$ and lies close to the diffraction pattern of an adjacent source which may affect the F140W photometry (Figure 1). UDF12-3895-7114 is the least secure with a 28% probability of lying at $z < 4$. We discuss UDF-3954-6284 below. Our deeper F105W data and the new F140W image also enables us to clarify the nature of $z > 8.5$ sources claimed in the earlier UDF09 analyses (see Table 1). In McLure et al. (2011)’s UDF09 analysis, no robust *J*-band dropout source was claimed (see also Bunker et al. 2010). However a solution with $z=8.49$ was found for HUDF_2003 which was also listed as the brightest extreme *Y*-band dropout in Bouwens et al. (2011) (ID: UDFy-38135539) who inferred a redshift $z \approx 8.7$ ¹⁰. Our new SED analysis indicates this source is at $z=8.3$. Similarly, two further extreme *Y*-band dropouts listed by Bouwens et al. (2011) - UDFy-37796000 and UDFy-33436598 at redshifts of $z \approx 8.5$ and 8.6 now lie at $z=8.0$ and 7.9, respectively. Bouwens et al. (2011) initially presented 3 sources as promising *J*-band dropouts (see Table 1). Two of these are detected in our deeper F105W data and lie at lower redshifts (UDFj-436964407 at $z=7.6$ and UDFj-35427336 at $z=7.9$, although $z \simeq 2$ solutions are also possible). One *Y*-band dropout in Bouwens et al. (2011), UDFy-39468075 moves into our sample at $z=8.6$. Finally, UDFj-38116243 claimed in the first year UDF09 data but later withdrawn by Bouwens et al. (2011) is below our 5σ detection limit. Yan et al. (2010) listed 20 potential *J*-band dropout candidates. Inspection of these revealed no convincing $z > 8.5$

¹⁰ This source was examined spectroscopically using the VLT SINFONI integral field spectrograph by Lehnert et al. (2010) who reported a detection of Ly α emission at $z=8.6$ but this claim is refuted by Bunker et al (in preparation) following a separate spectroscopic exposure with the higher resolution spectrograph X-shooter.

candidates; most appear as tails of bright objects and cannot be reliably photometered by SeXtractor. All of the ‘Y dropouts’ claimed by Lorenzoni et al. (2011) have robust F105W detections in our deeper data and lie below $z=8.5$.

In summary, only one object claimed to be at $z > 8.5$ from the earlier UDF09 analysis remains and that is the final *J*-band dropout presented by Bouwens et al. (2011) at $z=10.3$, UDFj-39546284 (\equiv UDF12-3954-6384 in Table 1). However, its non-detection in the UDF12 F140W data indicates a yet higher redshift of $z=11.9$ (Figure 2). The most significant advance of our campaign is a significant increase (from 0 to 6) in the number of robustly determined UDF sources in the redshift range $8.5 < z < 10$.

2.1. Contamination from Strong Emission Line Sources?

A major motivation for the additional F140W filter in our UDF12 strategy was to ensure the robust detection in two filters of potential $8.5 < z < 11.5$ candidates since the flux above 1216 \AA would be visible in both filters. This is the case for all but one of our UDF12 candidates (Table 1). A major surprise is the non-detection in F140W of UDFj-30546284 implying a redshift of $z=11.90$ (Figures 1 and 2).

Single band detections are naturally less convincing, although UDFj-30546284 is confirmed in F160W sub-exposures through UDF09 and UDF12, leaving no doubt it is a genuine source. However, an alternative solution must also be carefully considered. The sharp drop implied by the F140W - F160W > 1.5 (2σ) color precludes any reasonable foreground continuum source (Figure 2) but a possible explanation might be the presence of a very strong emission line. Recent WFC3/IR imaging and grism spectroscopy of $z \simeq 2$ galaxies has revealed a population of extreme emission line galaxies (EELGs). van der Wel et al. (2011) have identified an abundant population of EELGs at $z \simeq 1.7$ in the CANDELS survey using purely photometric selection techniques. Spectroscopy of a subset has verified the presence of sources with rest-frame [O III] equivalent widths up to $\simeq 1000 \text{ \AA}$. Independently, Atek et al. (2011) located a similar population in the WISP survey over $0.35 < z < 2.3$ and comment specifically that such sources could contaminate dropout searches.

Following techniques described in Robertson et al. (2010a) and Ono et al. (2010), we have simulated model spectra for young low metallicity dust-free galaxies including the contribution from strong nebular lines. Figure 3a shows the expected F105W - F160W color as a function of redshift for starbursts with ages of 1 and 10 Myr demonstrating that it is not possible to account for the significant excess flux in F160W from either intense [O II] 3727 \AA at $z \simeq 3.4$ or [O III] 5007 \AA at $z \simeq 2.4$. Figure 3b illustrates, for the case of intense [O III] emission that the expected stellar plus nebular emission spectrum of a 10 Myr starburst would violate the photometric flux limits provided by the various ACS and WFC3/IR broad band non-detections. If all of the emission in F160W arises from [O III] above a blue $\beta=2$ stellar continuum, the rest-frame equivalent width would have to be $> 4500 \text{ \AA}$, beyond that of any known object. A further difficulty is the absence of the expected Lyman α emission following a recent Keck optical spectrum (Figure 3b). However, although we can find no physically self-consistent starburst model that can simultaneously explain

the F160W emission and satisfy our upper limits in Figure 3b, only an infrared spectrum would completely eliminate the possibility of some exotic foreground emission line source. As the source has $H_{AB}=29.3$, this would be a very challenging observation. For the remainder of the paper we will interpret this source with caution.

3. THE ABUNDANCE OF GALAXIES WITH $8.5 < Z < 12$

A key issue is whether the declining cosmic star formation which is now well-established over $6 < z < 8$ (Bouwens et al. 2007) continues to higher redshift as suggested by the presence of evolved stellar populations with ages of $\simeq 200\text{-}300$ Myr at $z \simeq 5\text{-}7$ (e.g., Richard et al. 2011). Bouwens et al. (2011) claimed, from their detection of apparently only one object at $z \simeq 10$ c.f. three expected, that the star formation history declines more steeply beyond $z \simeq 8$ (see also Oesch et al. 2012) to $\dot{\rho}_*(z \sim 10) \approx 2 \times 10^{-4} M_{\odot} \text{ yr}^{-1} \text{ Mpc}^{-3}$. Recently, the CLASH survey has located several $z > 8.5$ candidates (Coe et al. 2012) implying star formation rate densities higher than claimed by Bouwens et al. (2011) at $z \sim 10$. However, the uncertain search volumes inherent in the lensing method are a major concern.

In Figure 4 we present the implications of the significant increase in the number of $8.5 < z < 12$ sources arising from the UDF12 campaign. Our SED-based selection method enables us to consider separately four redshift bins. As a direct determination of the luminosity function at $z > 8.5$ is not yet possible, to estimate the UV luminosity densities for our four detections at $8.5 \lesssim z < 9.5$ we calculate the required redshift evolution in the characteristic luminosity dM_*/dz such that a survey of our depth and selection efficiency would recover the number of sources we find. This calculation is performed assuming simple luminosity evolution from $z \sim 8$, keeping the luminosity function normalization ϕ_* and faint-end slope α fixed at the $z \sim 8$ values measured by Bradley et al. (2012). To reproduce our sample with mean redshift $\langle z \rangle \approx 8.9$, we find that $dM_*/dz \approx 1.09$. The luminosity density can then be estimated by integrating the projected luminosity function parameters to $M_{UV} \approx -17.7 \text{ AB}$ (e.g., Bouwens et al. 2011; Coe et al. 2012; Bouwens et al. 2012b). We find $\rho_{UV}(z \sim 8.9) \approx 1.08 \times 10^{25} \text{ ergs s}^{-1} \text{ Hz}^{-1} \text{ Mpc}^{-3}$ (Figure 4, blue point). A similar calculation provides $\rho_{UV}(z \sim 9.8) \approx 7.89 \times 10^{24} \text{ ergs s}^{-1} \text{ Hz}^{-1} \text{ Mpc}^{-3}$ from the two $z \sim 9.5$ detections (magenta point). The expected UDF cosmic variance for $8.5 \lesssim z \lesssim 9.5$ is $> 40\%$ (Robertson 2010b). Within $10.5 \lesssim z \lesssim 11.5$, we find no candidates. Nonetheless we can use the same methodology to provide an upper limit of $\rho_{UV}(z \sim 10.8) < 9.57 \times 10^{24} \text{ ergs s}^{-1} \text{ Hz}^{-1} \text{ Mpc}^{-3}$ (Figure 4, purple upper limit).

Considering the putative $z \sim 12$ source, both its morphology (Figure 1) and its luminosity cause us to be cautious, particularly given the paucity of other detections beyond $z \simeq 10.5$. Nonetheless, since the emission line hypothesis is equally difficult to accept (Section 2.1), we estimated the luminosity density using only the source luminosity ($M_{UV} = -19.6 \text{ AB}$ accounting for IGM absorption in F160W, or $\log_{10} L_{UV} = 28.48 \log_{10} \text{ ergs s}^{-1} \text{ Hz}^{-1}$) and the UDF survey volume $V(11.5 \lesssim z \lesssim 12.5) = 6.37 \times 10^3 \text{ Mpc}^3$. The resulting luminosity density $\rho_{UV}(z \sim 11.8) > 4.7 \times$

10^{24} ergs s⁻¹ Hz⁻¹Mpc⁻³ is thus a lower limit (Figure 4, red point), and conservatively does not include multiplicative effects of selection efficiency or involve extrapolations from the $z \sim 8$ luminosity function. An additional possibility is that the F160W is contaminated by Ly α emission. The additional $z=12$ point (yellow) illustrates how this limit would be affected for a rest-frame equivalent width of 260 Å of which half is absorbed by neutral hydrogen.

In summary, the new galaxy sample provided by UDF12 has enabled us to present the first meaningful estimate of $\rho_{UV}(z)$ beyond $z \simeq 8.5$. The six galaxies with $8.5 < z < 10$ indicate a modest shortfall in $\rho_{UV}(z)$ beyond a simple extrapolation of the trend at $6 < z < 8$ (less sharp than that suggested by Bouwens et al. (2011), but below (albeit consistent with) the cluster results (Zheng et al. 2012; Coe et al. 2012)). However, if UDFj-30546284 is genuinely a $z=12$ galaxy (and does not have substantial Lyman- α emission) then we have witnessed an even more measured decline in $\rho_{UV}(z)$ to the highest redshift yet probed.

4. DISCUSSION

The UDF12 data has demonstrated the continued effectiveness of HST to undertake a census of very high redshift galaxies. Our discovery of the first robust sample of galaxies with $z > 8.5$ and possibly the most distant galaxy at $z \sim 12$ extends HST's reach further into the reionization epoch than previously thought possible (c.f., Bouwens et al. 2011). While the question of whether star-forming galaxies were solely responsible for reionizing intergalactic hydrogen is more reliably addressed through precise constraints on the $z \sim 7 - 8$ luminosity function

faint end slope (Schenker et al. 2012; McLure et al. 2012, see Robertson et al. 2012) this work has placed the first constraint on the SFR density only 360 million years after the Big Bang. Evidence for actively star-forming galaxies significantly beyond the instantaneous reionization redshift $z_{\text{reion}} \approx 10.6 \pm 1.2$ implied by observations of the cosmic microwave background (Komatsu et al. 2011) motivates future observations with *James Webb Space Telescope*. Our estimate of the $z \sim 10$ star formation rate densities are consistent with previous analyses aimed at explaining the measured Thomson optical depth (e.g. Robertson et al. 2010a; Kuhlen & Faucher-Giguère 2012) and that required to produce the stellar masses of $z < 8$ sources observed by *Spitzer* (e.g., Stark et al. 2012; Labbé et al. 2012). Our results remain consistent with the simple picture for the evolving star formation rate density, stellar mass density, Thomson optical depth, and IGM ionization fraction presented in Robertson et al. (2010a).

US authors acknowledge financial support from the Space Telescope Science Institute under award HST-GO-12498.01-A. JSD acknowledges support of the European Research Council and the Royal Society. RJM acknowledges funding from the Leverhulme Trust. We thank Kimihiko Nakajima for assistance with the Keck spectroscopy. This work is based on data from the *Hubble Space Telescope* operated by NASA through the Space Telescope Science Institute via the association of Universities for Research in Astronomy, Inc. under contract NAS5-26555.

REFERENCES

- Atek, H., et al. 2011, ApJ, 743, 121
 Bouwens, R. J., Illingworth, G. D., Franx, M., & Ford, H. 2007, ApJ, 670, 928
 —. 2010, ApJ, 709, L133
 Bouwens, R. J., et al. 2011, Nature, 469, 504
 —. 2012a, ApJ, 752, L5
 —. 2012b, ArXiv: 1211.2230
 Bradley, L. D., et al. 2012, arXiv:1204.3937
 Bromm, V., & Yoshida, N. 2011, ARA&A, 49, 373
 Bunker, A. J., et al. 2010, MNRAS, 409, 855
 Calzetti, D., Armus, L., Bohlin, R. C., Kinney, A. L., Koornneef, J., & Storchi-Bergmann, T. 2000, ApJ, 533, 682
 Coe, D., et al. 2012, submitted
 Dunlop, J. S. 2012, ArXiv: 1205.1543
 Dunlop, J. S., et al. 2012, in preparation
 Ellis, R., Santos, M. R., Kneib, J.-P., & Kuijken, K. 2001, ApJ, 560, L119
 Eyles, L. P., Bunker, A. J., Ellis, R. S., Lacy, M., Stanway, E. R., Stark, D. P., & Chiu, K. 2007, MNRAS, 374, 910
 González, V., Labbé, I., Bouwens, R. J., Illingworth, G., Franx, M., & Kriek, M. 2011, ApJ, 735, L34
 González, V., Labbé, I., Bouwens, R. J., Illingworth, G., Franx, M., Kriek, M., & Brammer, G. B. 2010, ApJ, 713, 115
 Kneib, J.-P., Ellis, R. S., Santos, M. R., & Richard, J. 2004, ApJ, 607, 697
 Koekemoer, A., et al. 2012, in preparation
 Komatsu, E., et al. 2011, ApJS, 192, 18
 Kuhlen, M., & Faucher-Giguère, C.-A. 2012, MNRAS, 423, 862
 Labbe, I., et al. 2012, ArXiv e-prints
 Lehnert, M. D., et al. 2010, Nature, 467, 940
 Lorenzoni, S., et al. 2011, MNRAS, 414, 1455
 Madau, P., Pozzetti, L., & Dickinson, M. 1998, ApJ, 498, 106
 McLure, R. J., Dunlop, J. S., Cirasuolo, M., Koekemoer, A. M., Sabbi, E., Stark, D. P., Targett, T. A., & Ellis, R. S. 2010, MNRAS, 403, 960
 McLure, R. J., et al. 2011, MNRAS, 418, 2074
 McLure, R.J., et al. 2012, in preparation
 Oesch, P. A., et al. 2010, ApJ, 709, L16
 —. 2012, ApJ, 745, 110
 Oke, J. B., 1974 ApJS, 27, 21
 Ono, Y., Ouchi, M., Shimasaku, K., Dunlop, J., Farrah, D., McLure, R., & Okamura, S. 2010, ApJ, 724, 1524
 Richard, J., Kneib, J.-P., Ebeling, H., Stark, D. P., Egami, E., & Fiedler, A. K. 2011, MNRAS, 414, L31
 Robertson, B. E., Ellis, R. S., Dunlop, J. S., McLure, R. J., & Stark, D. P. 2010, Nature, 468, 49
 Robertson, B. E. 2010, ApJ, 713, 1266
 Robertson, B., et al. 2012, in preparation
 Santos, M. R., Ellis, R. S., Kneib, J.-P., Richard, J., & Kuijken, K. 2004, ApJ, 606, 683
 Schenker, M., et al. 2012, in preparation
 Shapley, A. E., Steidel, C. C., Pettini, M., & Adelberger, K. L. 2003, ApJ, 588, 65
 Stark, D. P., Bunker, A. J., Ellis, R. S., Eyles, L. P., & Lacy, M. 2007a, ApJ, 659, 84
 Stark, D. P., Ellis, R. S., Richard, J., Kneib, J.-P., Smith, G. P., & Santos, M. R. 2007b, ApJ, 663, 10
 Stark, D. P., Schenker, M. A., Ellis, R. S., Robertson, B., McLure, R., & Dunlop, J. 2012, ArXiv e-prints
 van der Wel, A., et al. 2011, ApJ, 742, 111
 Yan, H.-J., Windhorst, R. A., Hathi, N. P., Cohen, S. H., Ryan, R. E., O'Connell, R. W., & McCarthy, P. J. 2010, Research in Astronomy and Astrophysics, 10, 867
 Zheng, W., et al. 2012, Nature, 489, 406

TABLE 1
 $z > 8.5$ Candidates

ID	RA	Dec	$z_{\text{SED}}(\pm 1\sigma)$	Y_{105W}	J_{125W}	J_{140W}	H_{160W}	Notes
UDF12 Survey Depth 5-σ AB (aperture diameter arcsec - 70% enclosed point source flux)								
				30.0 (0.40)	29.5 (0.44)	29.5 (0.47)	29.5 (0.50)	
UDF12 Galaxies^a								
UDF12-3954-6284	3:32:39.54	-27:46:28.4	$11.9^{+0.3}_{-0.5}$	> 31.2	> 30.7	> 30.5	29.3 ± 0.2	UDFj-39546284 B11 ^b
UDF12-4106-7304	3:32:41.06	-27:47:30.4	$9.5^{+0.4}_{-0.8}$	> 30.8	> 30.0	29.8 ± 0.3	29.7 ± 0.3	
UDF12-4265-7049	3:32:42.65	-27:47:04.9	$9.5^{+0.4}_{-0.7}$	> 31.2	30.4 ± 0.6	29.9 ± 0.4	29.7 ± 0.4	
UDF12-3921-6322	3:32:39.21	-27:46:32.2	$8.8^{+0.4}_{-0.2}$	> 31.2	29.9 ± 0.3	29.6 ± 0.3	29.9 ± 0.3	
UDF12-4344-6547	3:32:43.44	-27:46:54.7	$8.8^{+0.5}_{-0.5}$	> 31.2	30.0 ± 0.3	30.1 ± 0.4	30.1 ± 0.3	
UDF12-3895-7114	3:32:38.95	-27:47:11.4	$8.6^{+0.8}_{-0.6}$	> 30.9	30.4 ± 0.5	30.1 ± 0.3	30.1 ± 0.4	
UDF12-3947-8076	3:32:39.47	-27:48:07.6	$8.6^{+0.2}_{-0.2}$	31.0 ± 0.5	29.5 ± 0.2	29.0 ± 0.1	29.0 ± 0.1	UDFy-39468075 B11 ^b
Earlier Candidates^a								
UDFj-39546284	3:32:39.54	-27:46:28.4	$11.9^{+0.3}_{-0.5}$	> 31.2	> 30.7	> 30.5	29.3 ± 0.2	B11 ^b $z \simeq 10.3$
UDFj-38116243	3:32:38.11	-27:46:24.3	—	> 31.2	> 30.1	30.3 ± 0.5	30.0 ± 0.3	B UDF09 ^c #1, B11 ^b #2
UDFj-43696407	3:32:43.69	-27:46:40.7	$7.6^{+0.4}_{-0.6}$	31.0 ± 0.6	> 30.1	29.9 ± 0.3	29.5 ± 0.2	B UDF09 ^c #2
UDFj-35427336	3:32:35.42	-27:47:33.6	$7.9^{+0.9}_{-0.8}$	> 30.8	30.3 ± 0.4	30.2 ± 0.4	29.6 ± 0.2	B UDF09 ^c #3
UDFy-38135539	3:32:38.13	-27:45:53.9	$8.3^{+0.2}_{-0.1}$	30.1 ± 0.2	28.6 ± 0.1	28.5 ± 0.1	28.4 ± 0.1	B11 ^b $8.5 < z < 9.5$
UDFy-37796000	3:32:37.79	-27:46:00.0	$8.1^{+0.1}_{-0.2}$	29.8 ± 0.1	28.6 ± 0.1	28.7 ± 0.1	28.7 ± 0.1	B11 ^b $8.5 < z < 9.5$
UDFy-33436598	3:32:33.43	-27:46:59.8	$7.9^{+0.2}_{-0.3}$	30.3 ± 0.4	29.3 ± 0.2	29.4 ± 0.2	29.4 ± 0.1	B11 ^b $8.5 < z < 9.5$

^a Upper photometric limits are 2σ .

^b Bouwens et al. (2011)

^c Bouwens et al. UDF09 yr. 1

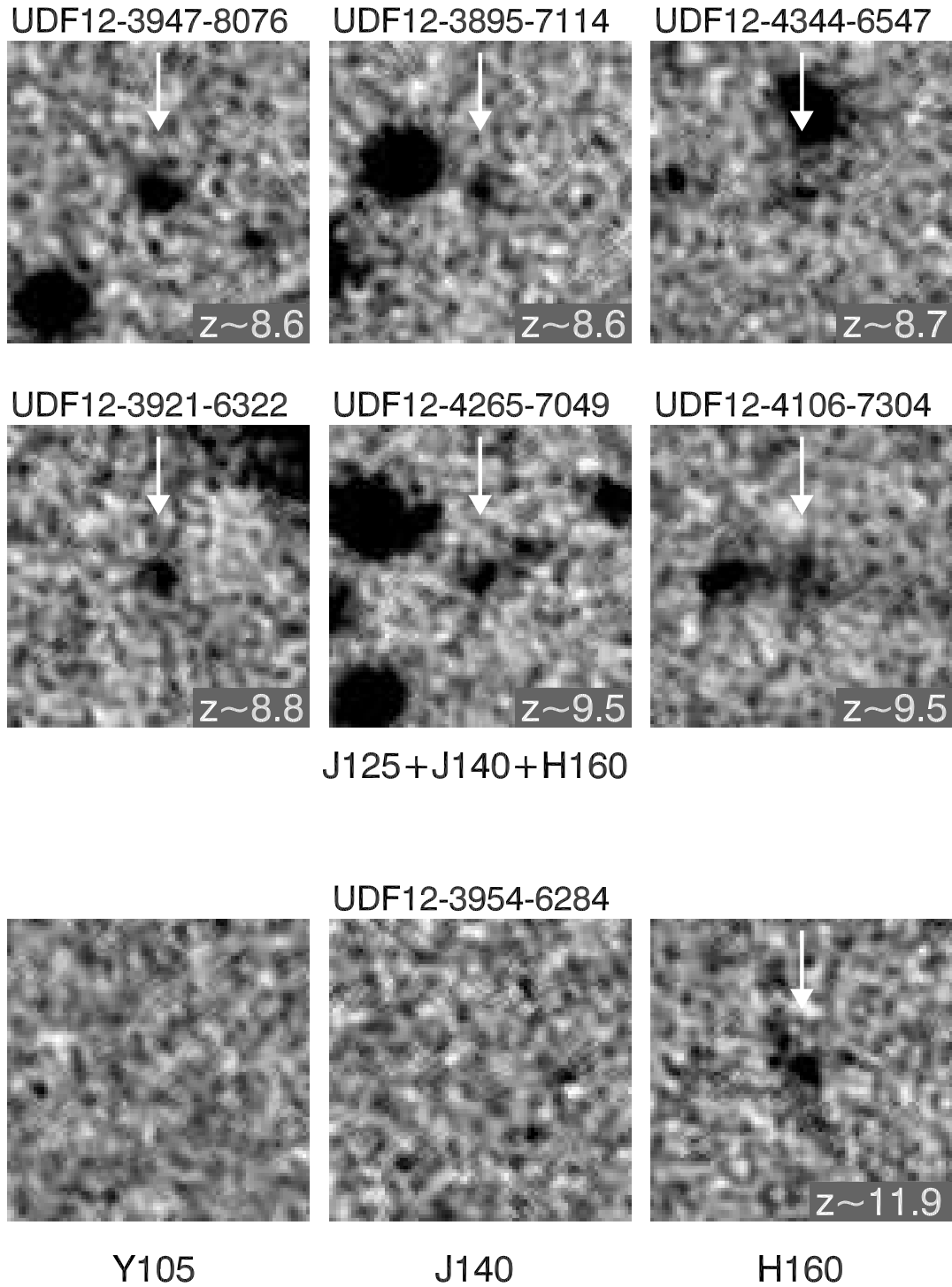


FIG. 1.— Hubble Space Telescope WFC3/IR images of the promising $z > 8.5$ candidates from combined UDF12 and earlier data. Each panel is 2.4 arcsec on a side. (Top two rows) Summed (F125W+F140W+F160W) images for 6 sources with $8.5 < z < 10.0$. (Bottom row) F105W, F140W, F160W images for UDF12-3954-6284 \equiv UDFj-39546284.

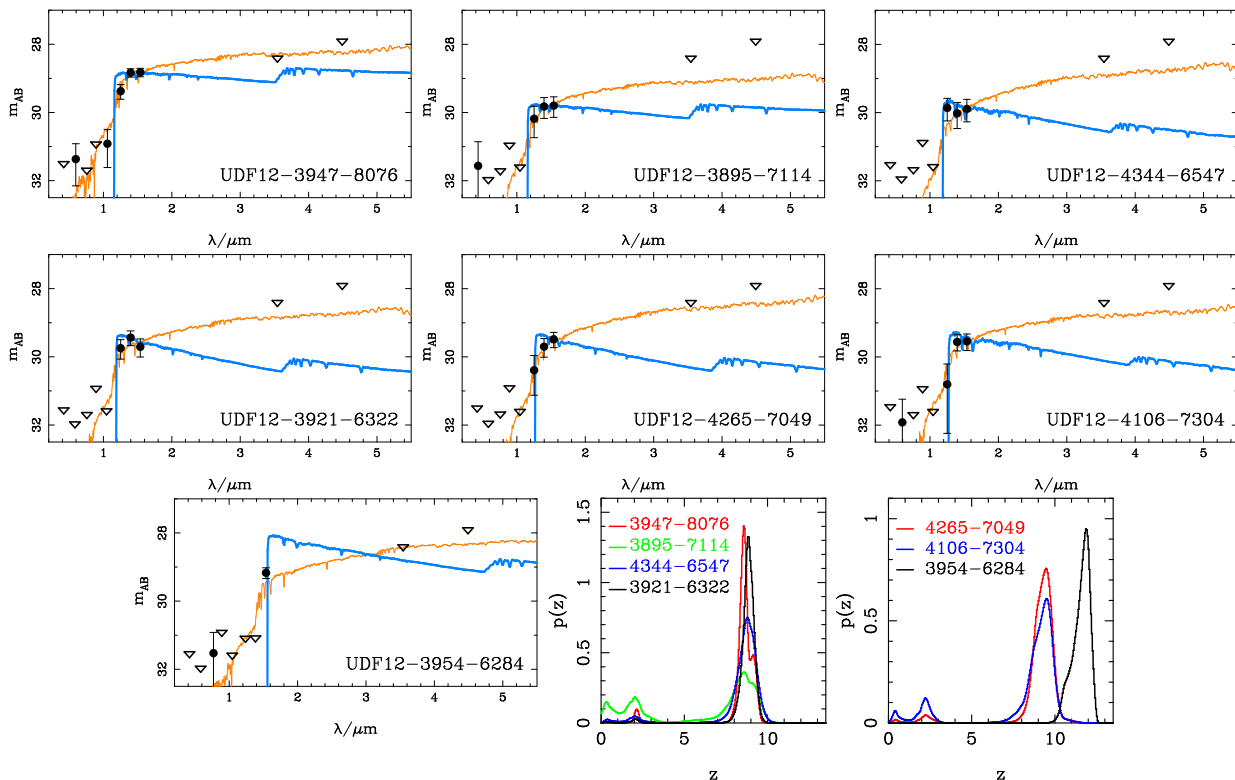


FIG. 2.— Spectral energy distributions for 7 promising $z > 8.5$ candidates from combined UDF12 and earlier data. Blue lines represent the adopted high z solution, orange lines the best rejected low z alternative. Upper limits are $1\text{-}\sigma$. IRAC limits of $m_{3.6} > 28.5$ and $m_{4.5} > 28.0$ are based on a deconvolution analysis of the Labbé et al. (2012) data using the UDF12 H_{160} image and the technique described in McLure et al. (2011). The final two panels show photometric likelihood fits for the sub-samples with $8.5 < z < 9.5$ and $z \geq 9.5$.

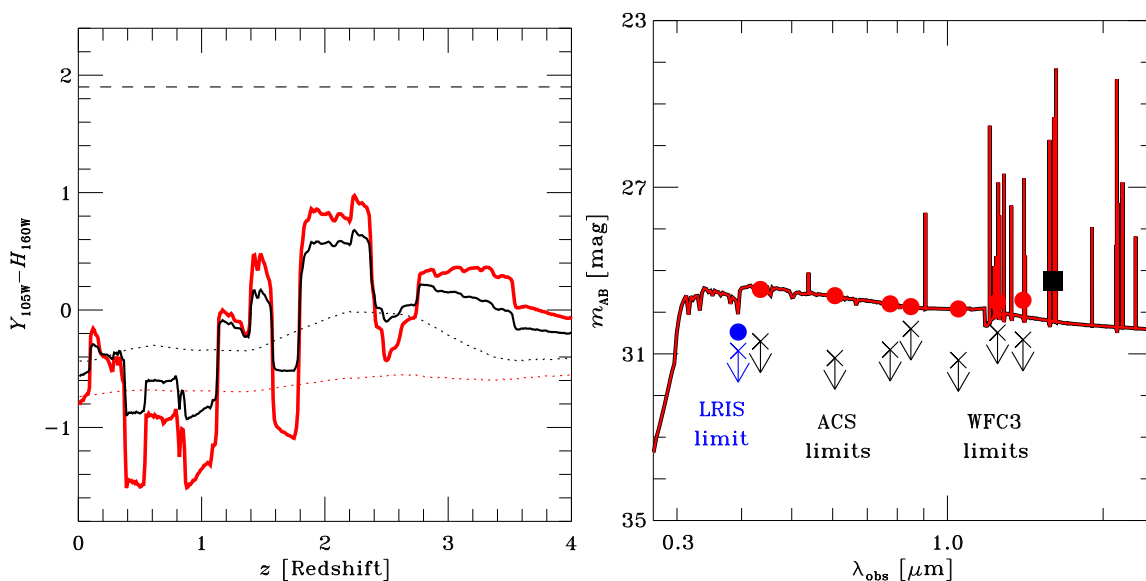


FIG. 3.— Possible contamination by foreground extreme emission line galaxies. (Left) F105W minus F160W color as a function of redshift for a 1 Myr (red) and 10 Myr (black) metal-poor dust-free stellar population incorporating nebular emission following the precepts of Ono et al (2010). Expectations for a stellar continuum only are shown by the dotted lines. The upper dashed line is the lower limit for UDFj-39546284 derived from the 2σ F105W limit and the $>6\sigma$ F160W detection. (Right). Simulated spectrum of UDFj-39546284 assuming a 10 Myr starburst at $z=2.24$ where [O III] emission dominates the F160W signal. Arrows indicate 2σ upper limits from non-detections in the various WFC3/IR and ACS bands. The blue circle indicates the expected Lyman α strength rejected by a Keck spectrum (blue arrow).

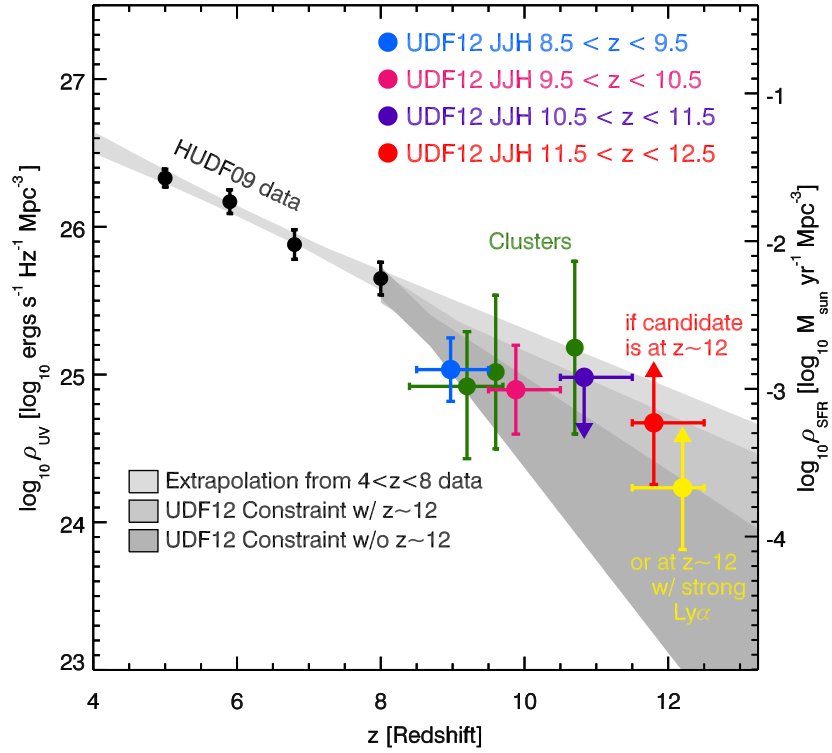


FIG. 4.— Luminosity and star formation rate (SFR) density versus redshift inferred from UDF12. Reddening corrected luminosity densities are shown from Bouwens et al. (2007, 2011) over the redshift range $5 < z < 8$ (black points). Extrapolating their evolution to redshift $z \sim 13$ provides the lightest gray area. Claimed estimates from the CLASH detections (green points) (Zheng et al. 2012; Coe et al. 2012; Bouwens et al. 2012b) are shown. Luminosity densities are shown for the four $8.5 \lesssim z \lesssim 9.5$ sources (blue data point) and the two $9.5 \lesssim z \lesssim 10.5$ objects (magenta point). The nondetection at $10.5 \lesssim z \lesssim 11.5$ provides an upper limit at $z \approx 10.8$ (purple limit). The single $z \sim 12$ source provides a conservative lower limit at $z \approx 11.8$ (red point). If this source has strong $\text{Ly}\alpha$ emission, the luminosity density limit becomes the yellow point. Overlapping maximum likelihood 68% confidence regions on a linear trend in the luminosity density with redshift from $z \sim 8$ are shown with (medium gray) and without (dark gray) the $z \sim 12$ object. The luminosity density computation is described in Section 3. Associated star formation rates (right axis) were calculated using the conversion of Madau et al. (1998).